THE JOURNAL OF BIOLOGICAL CHEMISTRY VOL. 287, NO. 47, pp. 39513–39523, November 16, 2012

Hyperactivity of the Ero1α Oxidase Elicits Endoplasmic Reticulum Stress but No Broad Antioxidant Response[S]

Received for publication, July 26, 2012, and in revised form, September 28, 2012 Published, JBC Papers in Press, October 1, 2012, DOI 10.1074/jbc.M112.405050

Henning Gram Hansen[‡1], Jonas Damgård Schmidt[‡], Cecilie Lützen Søltoft[‡], Thomas Ramming[§2], Henrik Marcus Geertz-Hansen[¶‖], Brian Christensen[‡‡], Esben Skipper Sørensen[‡‡], Agnieszka Sierakowska Juncker[¶‖], Christian Appenzeller-Herzog[‡§3], and Lars Ellgaard[‡4]**

*From the [‡]Department of Biology, University of Copenhagen, 2200 Copenhagen N., Denmark, the [§]Department of Pharmaceutical Sciences, University of Basel, 4056 Basel, Switzerland, [¶]Center for Biological Sequence Analysis, Department of Systems Biology, Technical University of Denmark, 2800 Kgs. Lyngby, Denmark, [‖]Novo Nordisk Foundation Center for Biosustainability, Technical University of Denmark, 2970 Hørsholm, Denmark, **Novozymes A/S, 2800 Bagsværd, Denmark, and the [‡‡]Protein Chemistry Laboratory, Department of Molecular Biology and Genetics, Aarhus University, 8000 Aarhus, Denmark*

Background: The oxidase activity of human Ero1α generates hydrogen peroxide in the ER.
Results: Overexpression of a hyperactive Ero1α mutant induces the unfolded protein response but does not cause a broad antioxidant response.
Conclusion: Ero1α hyperactivity elicits ER stress through local ER lumenal hyperoxidation.
Significance: These findings show how the cell negotiates oxidative stress generated specifically in the lumen of the ER.

Oxidizing equivalents for the process of oxidative protein folding in the endoplasmic reticulum (ER) of mammalian cells are mainly provided by the Ero1α oxidase. The molecular mechanisms that regulate Ero1α activity in order to harness its oxidative power are quite well understood. However, the overall cellular response to oxidative stress generated by Ero1α in the lumen of the mammalian ER is poorly characterized. Here we investigate the effects of overexpressing a hyperactive mutant (C104A/C131A) of Ero1α. We show that Ero1α hyperactivity leads to hyperoxidation of the ER oxidoreductase ERp57 and induces expression of two established unfolded protein response (UPR) targets, BiP (immunoglobulin-binding protein) and HERP (homocysteine-induced ER protein). These effects could be reverted or aggravated by *N*-acetylcysteine and buthionine sulfoximine, respectively. Because both agents manipulate the cellular glutathione redox buffer, we conclude that the observed effects of Ero1α-C104A/C131A overexpression are likely caused by an oxidative perturbation of the ER glutathione redox buffer. In accordance, we show that Ero1α hyperactivity affects cell viability when cellular glutathione levels are compromised. Using microarray analysis, we demonstrate that the cell reacts to the oxidative challenge caused by Ero1α hyperactivity by turning on the UPR. Moreover, this analysis allowed the identification of two new targets of the mammalian UPR, CRELD1 and c18orf45. Interestingly, a broad antioxidant response was not induced. Our findings suggest that the hyperoxidation generated by Ero1α-C104A/C131A is addressed in the ER lumen and is unlikely to exert oxidative injury throughout the cell.

In eukaryotic cells, formation of structural disulfide bonds takes place in the lumen of the endoplasmic reticulum (ER)[5] and is an essential step in the folding of many proteins of the secretory pathway. The flavoproteins of the ER oxidoreductin-1 (Ero1) protein family are the main source of *de novo* generated disulfide bonds in human cells (1, 2) where two paralogs of Ero1 exist: Ero1α and Ero1β (3, 4). Whereas Ero1β is only present in select tissues (4, 5), Ero1α is widely expressed (4). Both enzymes oxidize the active-site cysteines of certain protein disulfide isomerases (PDIs), which in turn introduce disulfide bonds into newly synthesized proteins (6–8). In the catalytic cycle of Ero1 enzymes, the so-called outer active site oxidizes the PDI by disulfide exchange. The electrons received from the PDI are then shuffled to the inner active site of Ero1 and onto the adjacent flavin adenine dinucleotide cofactor. The ultimate electron acceptor is molecular oxygen. As a result, Ero1α and -β generate the reactive oxygen species (ROS) hydrogen peroxide (H_2O_2) (8–10). Thus, Ero1 activity must be regulated to prevent ROS build-up and hyperoxidizing conditions in the ER (11).

[S] This article contains supplemental Tables S1–S3.
The microarray data have been deposited with the NCBI gene expression and hybridization array data repository (Gene Expression Omnibus (GEO)) under the accession number GSE40601.

[1] Supported by a shared Ph.D. scholarship from Lundbeckfonden and the Faculty of Science at the University of Copenhagen and a recipient of an EliteForsk Travel Stipend from the Danish Ministry of Science, Innovation, and Higher Education.
[2] Recipient of a Ph.D. fellowship from the Boehringer Ingelheim Fonds.
[3] Recipient of an Ambizione grant from the Swiss National Science Foundation.
[4] Supported by the Danish Council for Independent Research (Natural Sciences), Novo Nordisk Fonden, and by Lundbeckfonden. To whom correspondence should be addressed: Dept. of Biology, University of Copenhagen, Ole Maaløes Vej 5, 2200 Copenhagen N., Denmark. Tel.: 45-35321725; Fax: 45-35322128; E-mail: lellgaard@bio.ku.dk.

[5] The abbreviations used are: ER, endoplasmic reticulum; ERAD, ER-associated degradation; AMS, 4-acetamido-4′-maleimidylstilbene-2,2′-disulfonic acid; BiP, immunoglobulin-binding protein; BSO, L-buthionine-sulfoximine: CRELD1, cysteine-rich with EGF-like domain protein 1; dox, doxycycline; DTE, dithioerythritol; Ero1, endoplasmic reticulum oxidoreductin-1; GO, gene ontology; HERP, homocysteine-induced ER protein; IAM, iodoacetamide; NAC, *N*-acetylcysteine; NEM, *N*-ethylmaleimide; PDI, protein disulfide isomerase; ROS, reactive oxygen species; UPR, unfolded protein response; dox, doxycycline.

Intramolecular disulfide bonds have been shown to negatively regulate the activity of both human Ero1 paralogs (10, 12–14). Although the activity of Ero1α is tightly controlled (12–14), Ero1β seems to be more loosely regulated (10, 13). The disulfide pattern of Ero1β has been proposed based on mutational analysis and SDS-PAGE mobility (10). In Ero1α, the majority of disulfide bonds have been identified by mass spectrometry (13) and in the crystal structure (15) (see also Fig. 1*A*). Because of different arrangements of intramolecular disulfide bonds, monomeric Ero1α migrates as three distinct species (redox forms) by SDS-PAGE under non-reducing conditions: Red, OX1, and OX2 (5, 13, 16, 17). The latter is the most oxidized redox form, and with all the regulatory disulfides in place it constitutes the inactive state of the enzyme (13). The relative abundance of these redox forms in endogenous Ero1α can vary substantially (13).

The small thiol-containing molecule glutathione makes up the ER redox buffer by maintaining a closely balanced ratio of its oxidized (GSSG) and reduced (GSH) forms (18, 19). Although the GSSG:GSH ratio is higher (more oxidizing) in the secretory pathway relative to the cytosol (20), a principal role of the glutathione redox couple in the ER is to maintain the redox state of PDIs sufficiently reduced to ensure efficient isomerization of non-native disulfide bonds (21, 22). The distribution of Ero1α redox forms is responsive to the GSSG:GSH ratio in the ER (22), although GSH is an inefficient substrate for oxidation by Ero1α (14, 23, 24). The equilibrium between the glutathione redox buffer and Ero1α is mediated by PDI, as the availability of reduced PDI influences the redox state of Ero1α (13). These interactions establish a feedback mechanism ensuring efficient and rapid homeostatic control of the ER redox state (1). A similar model for ER redox regulation has recently been demonstrated in *Saccharomyces cerevisiae*, with an additional layer of autonomous control demonstrated by the ability of yeast Ero1 (Ero1p) to self-oxidize regulatory cysteine residues in *trans* (25).

Non-optimal folding conditions in the ER, *e.g.* perturbation of the redox balance and increased ROS levels, can result in protein misfolding and thereby turn on the unfolded protein response (UPR) (26–28). The UPR is a coordinated transcriptional and translational program that is initiated by accumulation of misfolded proteins in the ER (designated as ER stress) (29). The UPR seeks to restore normal cellular conditions, for instance by up-regulating ER chaperones while *e.g.* also increasing ER-associated degradation (ERAD) of misfolded ER proteins (30). Failure of the cell to adapt to the stress condition eventually turns on proapoptotic pathways resulting in cell death (31).

Protein kinase RNA-like ER kinase (PERK), inositol-requiring protein 1α (IRE1α), and activating transcription factor 6α (ATF6α) constitute the three proximal UPR transducers that are activated upon ER stress (31). These transducers sense ER stress differentially, and their downstream target genes only partially overlap (32). For instance, the PERK branch is the only pathway shown to induce an antioxidant stress response (33, 34). In addition, ERAD is likely also implicated in negotiating oxidative stress by preventing ROS build-up (35). The close connection between protein misfolding, ROS, and the UPR is underscored by the finding that overexpression of a protein that misfolds in the ER can lead to the production of ROS and that these two factors (misfolded protein and ROS) together induce the UPR (36).

Professional secretory cells, such as antibody-producing plasma cells and insulin-producing β cells, produce large quantities of disulfide-bonded proteins, and the concomitant Ero1-generated H_2O_2 is presumed to pose a significant challenge to ER homeostasis (29). The overall cellular response to this challenge is unclear. Here, we show that overexpression of a hyperactive Ero1α mutant creates hyperoxidizing conditions in the ER and induces expression of two established UPR targets. The observed effects could be modulated by agents that manipulate the cellular glutathione redox buffer. The global transcriptional response to Ero1α hyperactivity revealed induction of the UPR, whereas a broad antioxidant response was conspicuously absent. Our results indicate that Ero1α hyperactivity elicits ER stress through local ER lumenal hyperoxidation.

EXPERIMENTAL PROCEDURES

Plasmids and Primers—Human Ero1α-myc6his (Ref. 3; a gift from R. Sitia, Milan) cloned into the pcDNA5/FRT/TO vector (13) was used as the template for QuikChange mutagenesis (Stratagene) to introduce Cys-to-Ala mutations. The following primers were used (only the sense strand is shown): C85A (5′-CCTGAAGAGGCCGGCTCCTTTCTGGAATGACATC-AGC-3′); C104A (5′-GGACTGTGCTGTCAAACCAGCTCAA-TCTGATGAAGTTCC-3′); C391A (5′-CAAGAATTATG-GATGCTGTTGGTTGTTTTAAATGTCG-3′). The C131A mutation has been described before (13). All plasmids were sequenced to confirm the correct DNA sequence of the inserts.

Cell Culture—Doxycycline (dox)-inducible Flp-In T-REx HEK-293 (Invitrogen) cell lines were generated as previously described (13). The cell lines were grown in α-minimal essential medium (Invitrogen), supplemented with 10% FCS, 100 μg/ml hygromycin B (Invitrogen), and 15 μg/ml blasticidin (Invivogen) at 37 °C, 5% CO_2. Ero1α expression was induced for 24 h (unless otherwise stated) using 1 μg/ml doxycycline (Sigma). Where indicated, cells were treated with 5 mM *N*-acetylcysteine (NAC; Sigma) for 18 h, which was added directly to the medium from a 250 mM stock dissolved in 100 mM HEPES (Invitrogen). Cells were treated with 1 mM buthionine sulfoximine (BSO; Sigma) dissolved in medium for the indicated periods of time. For ER stress induction, cells were treated with either 5 μM thapsigargin (Sigma) or 2.5 μg/ml tunicamycin (Sigma) for the indicated times.

Sample Preparation and 4-Acetamido-4′-maleimidylstilbene-2,2′-disulfonic acid (AMS) Modification—Cells were treated with *N*-ethyl-maleimide (NEM) and subsequently lysed as described elsewhere (37). The AMS (Invitrogen) modification protocol has been described previously (37). In brief, this protocol of differential alkylation with NEM and AMS results in modification of free cysteines with NEM, whereas those present in disulfides are decorated with AMS. Because of the size difference between the two alkylating agents, AMS modification gives rise to slower SDS-PAGE mobility compared with the NEM modification. Reduced and oxidized control lysates were

obtained from cells treated with 10 mM DTT or 5 mM diamide (both Sigma) for 5 min at 37 °C in full growth medium.

Antibodies—The following mouse monoclonal antibodies were used: αHis (Tetra-His, Qiagen), αmyc (9E10, Covance), αβ-actin (AC-15, Sigma). The rabbit polyclonal antisera used were: αBiP (G8918, Sigma), αERp57 (a gift from A. Helenius, Zürich, Switzerland), αHERP (a gift from L. Hendershot, Memphis, TN).

Western Blotting—All samples for Western blotting were separated by SDS-PAGE on Tris-glycine polyacrylamide Hoeffer minigels (GE Healthcare) before transfer onto a polyvinylidene difluoride membrane. Membranes were probed with primary antibodies in the following dilutions: ERp57, 1:1,000; β-actin, 1:25,000; homocysteine-induced ER protein (HERP), 1:2,000; immunoglobulin-binding protein (BiP), 1:5,000; myc, 1:1,000. After the addition of horseradish peroxidase-conjugated goat anti-rabbit or anti-mouse IgG (Pierce) secondary antibody, the bound antibody was detected with the ECL Prime detection reagent (GE Healthcare). All Western blots shown are representative of three independent experiments.

Metabolic Activity Assay—Cells were seeded in 24-well dishes at a density of 25,000 cells per well. After 24 h of incubation, cells were treated where indicated with 1 μg/ml doxycycline and/or 1 mM BSO for 48 h. As a positive control for cytotoxity, 5 μM thapsigargin was added for the last 20 h. The metabolic activity was then measured by incubating the cells in 400 μM water-soluble tetrazolium-1 (Santa Cruz Biotechnology) and 40 μM phenazine methosulfate (Sigma) in serum-reduced (1% FCS) medium for 30 min. The absorbance of hydrolyzed dye was then measured at 405 nm, and the background signal at 660 nm was subtracted. To ensure a linear relationship between the number of cells *versus* absorbance intensity, a 2-fold dilution series was made in each experiment. Statistical significance ($p \leq 0.05$) was assessed by performing Student's unpaired *t* test (two tailed, heteroscedastic) on log 2-transformed -fold changes.

Real-time Reverse-transcription PCR—RNA was extracted from cells using TRI Reagent (Sigma) according to the manufacturer's instructions. cDNA was synthesized by the RevertAid Premium Reverse Transcriptase (Fermentas) using poly-dT primers according to the manufacturer's guidelines. Real-time PCR reactions were performed on a CFX96 Real-time PCR Detection system (Bio-Rad) using the Power SYBR Green PCR Master Mix (Applied Biosystems). Gene specific primers are provided in the supplemental Table S1. The data were analyzed by the CFX manager software (Bio-Rad) and threshold cycle (Ct) values were used to compute the relative expression levels normalized to GAPDH using the $2(-\Delta\Delta C(T))$ method (38).

Array Analysis—Cells overexpressing Ero1α-WT and Ero1α-C104A/C131A were grown in triplicate, and expression was either not induced or induced with 1 μg/ml doxycycline for 24 h. RNA was extracted using TRI Reagent (Sigma) according to the manufacturer's instructions. The extracted RNA (250 ng) was amplified and labeled using the Ambion WT Expression kit (Applied Biosystems) according to the manufacturer's guidelines. The labeled samples were hybridized to the Human Gene 1.0 ST GeneChip array (Affymetrix, Santa Clara, CA). The arrays were washed and stained with phycoerythrin-conjugated streptavidin using the Affymetrix Fluidics Station® 450, and the arrays were scanned in the Affymetrix GeneArray® 3000 scanner to generate fluorescent images as described in the Affymetrix GeneChip® protocol. Cell intensity files (CEL files) were generated in the GeneChip® Command Console® Software (AGCC) (Affymetrix). The raw data were normalized, and the log 2-transformed expression indices were calculated using the robust multiarray average method (39) implemented in the statistical programming language R. Genes with significantly different expression levels between the four categories were identified by a two-way analysis of variance, where the cell line (Ero1α-WT or Ero1α-C104A/C131A) and induction status (−dox/+dox) were used as the two factors for the *p* value calculation. The number of top significant genes was selected based on estimations of false discovery rates obtained from *p* value calculation using balanced permuted categories. A *p* value threshold of 0.001 was selected as the cut-off. Log 2-transformed -fold changes (+dox/−dox) were calculated by computing the differences between the means of the log 2-transformed expression indices for both cell lines. Functional enrichment analysis with regard to gene ontology (GO) categories (biological process only) was performed using the Cytoscape plugin BiNGO (40). The threshold for the Fisher's exact test *p* values (corrected for multiple testing) was set to 0.01, and in case of several related significant GO terms only the most specific (the lowest child) was selected.

Disulfide Bridge Mapping—Ero1α was expressed and purified as previously described (13). Purified Ero1α was digested with sequencing grade-modified trypsin (Promega) at 37 °C overnight. Tryptic peptides were separated by reverse-phase HPLC on a μRPC C_2/C_{18} PC 2.1/10 column connected to an ÄKTA Explorer (GE Healthcare). Separation was carried out in 0.1% trifluoroacetic acid (buffer A) and eluted with a gradient of 80% acetonitrile in 0.1% trifluoroacetic acid (buffer B) developed over 95 min (0–5 min, 0% B; 5–90 min, 0–100% B; 90–95 min, 100% B) at a flow rate of 0.15 ml/min. The peptides were detected in the effluent by measuring the absorbance at 226 nm. All fractions were analyzed by MALDI-TOF-MS using a Voyager DE-PRO mass spectrometer (Applied Biosystems). The theoretical peptide masses were calculated using the GPMAW program (Lighthouse Data). For reduction of disulfide bond-containing peptides, the relevant HPLC fractions were dried in a vacuum centrifuge and then resuspended in 15 mM dithioerythritol (DTE) in 50 mM ammonium bicarbonate and incubated at 56 °C for 45 min. Free cysteines were alkylated by the addition of iodoacetamide (IAM) to 50 mM and incubated for 30 min in the dark at room temperature before characterization by MALDI-TOF-MS.

RESULTS

Cys^{104} Forms a Disulfide Bond with the Outer Active-site Cys^{99} in Ero1α OX2—The presence of a regulatory disulfide between Cys^{99} and Cys^{104} in human Ero1α has been proposed based on mutational analysis and previous investigations of the disulfide bond pattern in Ero1α (13, 14). Because Cys^{99} and Cys^{104} are located in a flexible loop, these residues were not observed in the crystal structure of the inactive OX2 form of

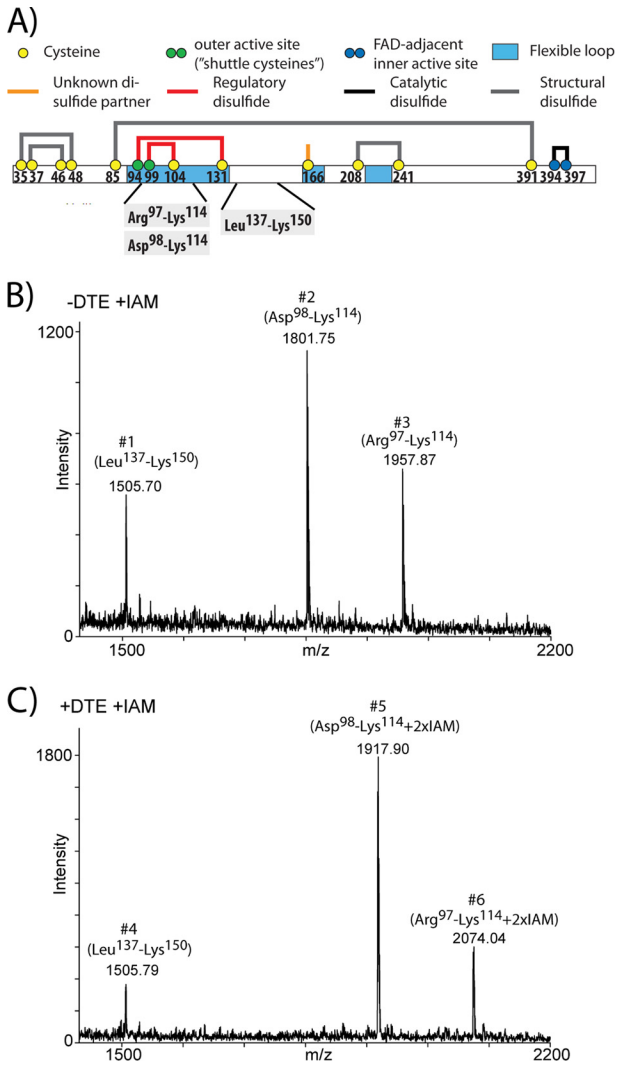

FIGURE 1. **Identification of the Cys^{99}–Cys^{104} disulfide bond in Ero1α.** *A*, shown is a schematic representation of the disulfide pattern in Ero1α OX2 based on (13, 15) and this study. The cysteine residues are shown as *yellow*, *green* (outer active site), or *blue* (inner active site) *circles* with amino acid numbering and disulfides as *thick gray* (likely structural), *black* (active site), or *red* (reported regulatory function based on Refs 12–14 and this study) lines. The *thick orange line* at Cys^{166} indicates the connection to a potential (but unidentified) disulfide partner. The flexible loop regions are colored in *light blue*. The three identified peptides after trypsin cleavage are shown in *gray boxes*. *B* and *C*, shown are mass spectra of Ero1α tryptic peptides treated with the alkylating agent IAM without prior reduction (*B*) or reduced with DTE and alkylated with IAM (*C*). Peak numbers are shown *above the peaks*. See "Results" and Table 1 for details.

Ero1α (15). Thus, direct experimental evidence for the presence of the Cys^{99}–Cys^{104} disulfide has been missing.

Affinity-tagged human Ero1α stably expressed in tissue-culture cells was purified in the OX2 redox state upon treatment with the alkylating agent NEM as previously described (13). The protein was digested with trypsin, and the resulting peptides were separated by HPLC and analyzed by mass spectrometry. The peptides were either left untreated or reduced with DTE and subsequently alkylated with IAM.

Peaks with masses corresponding to the oxidized forms of two tryptic peptides, Asp^{98}–Lys^{114} and Arg^{97}–Lys^{114} were detected in the non-reduced and IAM-treated material (peaks #2 and #3, respectively; Fig. 1*B* and Table 1). The differences between the observed masses for these two peptides and the theoretical monoisotopic masses for the corresponding reduced peptides were consistent with the presence of an intramolecular disulfide bond in both peptides (Table 1). No mass differences between the untreated material (−DTE-IAM; data not shown) and the non-reduced and IAM-treated material (−DTE+IAM) were observed, showing that the two tryptic peptides did not contain free thiol groups. When the peptides were reduced and alkylated, peaks #2 and #3 disappeared (Fig. 1*C* and Table 1). Instead, peaks #5 and #6 emerged corresponding to the Asp^{98}–Lys^{114} and Arg^{97}–Lys^{114} peptides, respectively, each decorated with two IAM moieties. This further supported the presence of an intramolecular disulfide bond in these two tryptic peptides. Because the Asp^{98}–Lys^{114} and Arg^{97}–Lys^{114} peptides only contain two cysteine residues (Cys^{99} and Cys^{104}), we concluded that these residues form a disulfide bond. The overall disulfide pattern of Ero1α OX2 is depicted in Fig. 1*A*.

Mutation of Cysteine Pairs Reveals Interplay between Sets of Disulfide Bonds—With the disulfide pattern at hand, we determined gel mobilities of specific Ero1α Cys-to-Ala mutants to analyze a potential interplay between the regulatory disulfides in Ero1α. Apart from already established stable cell lines for ectopic inducible expression of Ero1α-WT and Ero1α-C131A (13), we generated four new cell lines overexpressing the following mutants of Ero1α: C104A, C104A/131A, C85A/391A, and C85A/C104A/C131A/C391A. All six cell lines showed similar expression levels of Ero1α variants (Fig. 2*A*).

Exogenous Ero1α-WT migrated exclusively in the OX2 form (Fig. 2*B*, *lane 2*; see also Ref 13). Although the majority of C104A migrated like OX2, a small fraction migrated as OX1 (Fig. 2*B*, *lane 3*). This species likely lacks both of the regulatory disulfides, Cys^{94}–Cys^{131} and Cys^{99}–Cys^{104} (Fig. 2*C*). This suggested that the Cys^{94}–Cys^{131} disulfide was destabilized when the Cys^{99}–Cys^{104} disulfide did not form. As previously observed (13, 16), C131A migrated exclusively as OX1 (Fig. 2*B*, *lane 4*), which was also the case for C104A/C131A (Fig. 2*B*, *lane 5*). Whether removal of Cys^{94}–Cys^{131} destabilized the Cys^{99}–Cys^{104} bond could not be discerned because the absence of the Cys^{99}–Cys^{104} disulfide did not give rise to an apparent gel mobility shift (Fig. 2*B*, *lane 3*, *lower band*). Consistent with the previous observations for the single C85A and C391A mutants (16), Ero1α-C85A/C391A migrated as two distinct species (Fig. 2*B*, *lane 6*); one between the OX1 and OX2 forms and the other at the mobility of reduced Ero1α (*Red*). Although other possibilities cannot be excluded, the faster migrating species could contain an intact Cys^{94}–Cys^{131} disulfide, whereas this bond is resolved in the slower migrating species due to destabilization. On the contrary, the Cys^{85}–Cys^{391} disulfide did not seem to be destabilized by the lack of the Cys^{94}–Cys^{131} and/or Cys^{99}–Cys^{104} disulfides (Fig. 2*B*, *lanes 3–5*). It is unclear whether the Cys^{99}–Cys^{104} disulfide is present in Ero1α-C85A/C391A as its reduction would only give rise to a minimal mobility shift. Finally, Ero1α-C85A/C104A/C131A/C391A migrated exclusively as the red form. Taken together, the results showed that absence of certain disulfides influences the stability of others and that the Cys^{85}–Cys^{391} and Cys^{94}–Cys^{131} disulfides determine the three redox states of Ero1α-WT visible by SDS-PAGE.

TABLE 1
Mapping of the Cys^{99}–Cys^{104} disulfide bond in Ero1α

DTE[a]	IAM[a]	Peptides[b]	Cysteines[c]	Peak number[d]	Observed mass[e] (MH^+)	Mass difference[f] (MH^+)	Modification[g]
−	+	Arg^{97}–Lys^{114}	99, 104	#3	1957.87	−2.06	(1 S-S)
+	+	Arg^{97}–Lys^{114}	99, 104	#6	2074.04	114.11	(2 IAM)
−	+	Asp^{98}–Lys^{114}	99, 104	#2	1801.75	−2.08	(1 S-S)
+	+	Asp^{98}–Lys^{114}	99, 104	#5	1917.90	114.07	(2 IAM)
−	+	Leu^{137}–Lys^{150}		#1	1505.70	−0.04	
+	+	Leu^{137}–Lys^{150}		#4	1505.79	−0.05	

[a] Tryptic peptides were either left untreated or reduced with DTE and subsequently alkylated with IAM and analyzed by mass spectrometry.
[b] Tryptic peptides of Ero1α identified by MALDI-TOF-MS.
[c] Positions of cysteines contained in the identified peptides.
[d] Peak number as indicated in the spectra (Fig. 1, *B* and *C*).
[e] Observed monoisotopic molecular masses (MH^+) determined by MALDI-TOF-MS.
[f] Difference between observed masses and the theoretical masses of the reduced peptides.
[g] The number and type of modification corresponding to the mass difference: disulfide bridge (S-S) and alkylation with IAM.

In addition to the monomeric species of each Ero1α variant described above and consistent with previously published data (16), we also observed mixed disulfide complexes with endogenous PDI (data not shown). Judging from their gel mobilities, 1:1 complexes were formed for all variants. These migrated as distinct bands of slightly different mobilities depending on the specific variant of Ero1α involved. Similar complexes have recently been observed between mutants of Ero1p and endogenous Pdi1p (25). It was shown that cysteines of regulatory disulfide bonds in Ero1p were involved in forming the intermolecular disulfides to Pdi1p (25), and we suggest the same to occur in Ero1α. No Ero1α-containing high molecular weight aggregates were observed, suggesting that all five variants were correctly folded (see "Discussion").

Deregulated Ero1α Hyperoxidizes ERp57 and Induces the UPR—Recombinant Ero1α-C104A/C131A has been shown to be more active than Ero1α-WT and all other Ero1α mutants tested, as judged by faster consumption of molecular oxygen in an oxidase assay (12, 14, 15). Therefore, we chose to use Ero1α-WT and Ero1α-C104A/C131A for a comparison of the cellular response to regulated and deregulated Ero1α activity.

First, we compared the effect of inducing overexpression of Ero1α-WT and Ero1α-C104A/C131A on the cellular redox state of the PDI family member ERp57, as assessed by differential alkylation (see "Experimental Procedures") (13, 41). Expression of Ero1α-C104A/C131A clearly increased the oxidized fraction of ERp57 (Fig. 3*A*). In comparison to the Ero1α-C131A single mutant, Ero1α-C104A/C131A seemed to cause a more pronounced increase in hyperoxidation of ERp57, although the observed difference was only minor (data not shown). Consistent with previous studies (1, 7, 13), the redox distribution of ERp57 was only weakly affected by expression of Ero1α-WT. In parallel, we treated the cells with NAC, a cell-permeable glutathione precursor and widely used thiol-containing antioxidant (42) that increases the cellular level of GSH and thereby causes more reducing conditions (43, 44). In accordance, NAC treatment likely had a weak reducing effect on the redox state of ERp57 (Fig. 3*A*, *lane 9* and *10*). Interestingly, NAC addition partly reverted the oxidative shift on ERp57 caused by Ero1α-C104A/C131A expression (Fig. 3*A*, *lane 7* and *8*). No effect on the expression levels of Ero1α-WT and Ero1α-C104A/C131A was observed as a result of NAC treatment (Fig. 3*B*).

Next we studied a potential effect of the deregulated Ero1α mutant on two established UPR targets, HERP and BiP (45). Treatment of cells with tunicamycin and thapsigargin, two chemical inducers of the UPR, was used to generate positive controls. HERP and BiP protein levels were clearly increased by Ero1α-C104A/C131A but only weakly by Ero1α-WT overexpression (Fig. 3*C*). Moreover, NAC treatment abolished this effect (Fig. 3*C*). As NAC treatment did not have any effect on tunicamycin- and thapsigargin-induced ER stress as monitored by BiP and HERP expression (Fig. 3*D*, *lanes 3–6*), NAC did not seem to have a general inhibitory effect on UPR induction. HERP and BiP expression levels were also unaffected by treatment with NAC or doxycycline alone (Fig. 3*D*, *lanes 1* and *2* and *lanes 7* and *8*, respectively).

Ero1α-C104A/C131A Overexpression Affects Cell Viability Only When Cellular Glutathione Is Depleted—The results of NAC treatment indicated that the glutathione redox couple played an important role in buffering the effects of overexpressing Ero1α-C104A/C131A. To further investigate this possibility, we tested the effects of treating cells with BSO, an inhibitor of glutathione synthesis. As previously demonstrated for overexpression of Ero1α-C131A (13), the hyperoxidizing effect of Ero1α-C104A/C131A on ERp57 was clearly aggravated when treating cells with BSO (Fig. 4*A*).

Although cells overexpressing Ero1α-C104A/C131A for 24 h appeared to proliferate normally and visual inspection did not reveal any apparent abnormalities, unusual cell morphology could be observed after 48 h of induction, and this effect was aggravated by BSO treatment (data not shown). These impressions were confirmed in a water-soluble tetrazolium-1 assay, which measures the metabolic activity of mitochondrial dehydrogenases as readout for cell viability (Fig. 4*B*). Although overexpression of neither Ero1α-WT nor Ero1α-C104A/C131A for 48 h affected the metabolic activity, combining overexpression with BSO treatment resulted in a significant decrease only in cells overexpressing Ero1α-C104A/C131A. We concluded that overexpressing Ero1α-C104A/C131A affected viability only when cellular glutathione levels were compromised.

Global Transcriptional Response to Ero1α Hyperactivity—Having established that deregulation of Ero1α perturbs ER homeostasis, we next explored the global transcriptional response to this perturbation. RNA was extracted from cells not induced or induced to express Ero1α-WT and Ero1α-C104A/C131A with doxycycline for 24 h and subjected to microarray analysis using the Human Gene 1.0 ST GeneChip array. Principal component analysis of the data showed that the main vari-

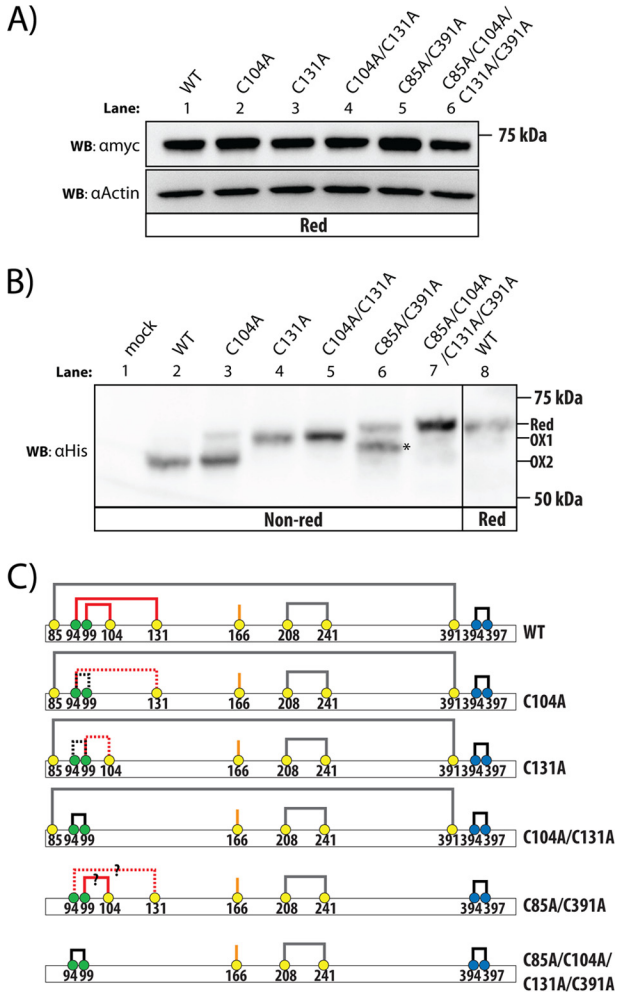

FIGURE 2. **The regulatory Cys^{94}–Cys^{131} disulfide in Ero1α is destabilized when the Cys^{99}–Cys^{104} disulfide is absent.** *A*, expression of His- and Myc-tagged Ero1 variants was induced with doxycycline for 24 h, and cells were NEM-treated to prevent post-lysis thiol-disulfide exchange reactions. Equal amounts of protein from lysates were analyzed by reducing SDS-PAGE and Western blotting (*WB*) using αMyc (Ero1α) and αActin (loading control) to compare expression levels of Ero1α variants. *B*, cell lysates were obtained as described for *A*, and the SDS-PAGE mobility of the Ero1α variants was analyzed under non-reducing (*Non-red*) or reducing (*Red*) conditions by αHis Western blotting. The mock cell line is stably transfected with an empty vector and functions as a background control. The *vertical hairline* denotes removal of one lane, and the *asterisk* indicates an uncharacterized redox form between OX1 and OX2. *C*, shown is a schematic representation of the proposed disulfide pattern (as in Fig. 1*A*) in the analyzed Ero1α Cys-to-Ala variants as inferred from gel mobility of monomeric species (see "Results" for details). For the sake of clarity, the N-terminal region until Cys-85 was omitted. A *dashed line* denotes the presence of the disulfide in only a fraction of the monomeric species, and a *question mark* indicates that the presence of the disulfide is unknown.

ation in the expression data was between the Ero1α-WT and the Ero1α-C104A/C131A cells regardless of the induction status (±dox; data not shown). Despite the transcriptional differences between the cell lines, we were able to identify a set of genes with significant changes due to expression of Ero1α-WT and Ero1α-C104A/C131A (±dox). This set contained 159 genes ($p < 0.001$, false discovery rate = 10%), and the majority of these (86.1%) were up-regulated (Fig. 5*A*, supplemental Table S2). For the 159 genes, overexpression of Ero1α-C104/131A clearly mediated more pronounced transcriptional changes compared with Ero1α-WT (Fig. 5*B*). Among the genes with GO cellular component annotations (122 of 159 genes), the majority of the corresponding gene products were ER-localized. In addition, a GO gene enrichment analysis of the 159 genes based on biological processes (115 genes had biological process GO annotations) was performed. This analysis showed a significant overrepresentation of genes involved in the UPR, ERAD, cell redox homeostasis, *N*-glycosylation, and negative regulation of caspase activity (data now shown).

When comparing log 2-transformed -fold changes (+dox/−dox) for the two Ero1α cell lines, a group of genes were identified to have considerably higher relative -fold changes between Ero1α-C104A/131A (+dox/−dox) and Ero1α-WT (+dox/−dox) (Fig. 5*C*). By setting the threshold to 0.3 for differences between log 2-transformed -fold changes, we identified a set of 26 genes with this particular expression profile (*above the dashed red line* in Fig. 5*C*), whereas no genes among the 159 genes had considerably lower relative -fold changes (*below the dashed blue line*). A GO enrichment analysis of these 26 genes (17 genes had biological process GO annotations) revealed significant over-representation of genes related to UPR, ERAD, redox homeostasis, and lipid biosynthesis (supplemental Table S3). Importantly, only one gene (SLC7A11) among the 109 genes of the GO term "Response to oxidative stress" (GO:0006979) was present among the 26 genes. Moreover, the same GO term was not among the significantly enriched biological process GO terms for the top 159 significant genes. Of the 109 genes in the above-mentioned GO term, only three (SELK, DHCR24, and SLC7A11) were detected in the set of 159 genes. The transcriptional response to Ero1α hyperactivity was, therefore, mainly addressed by a more pronounced UPR induction, whereas no apparent antioxidant response was induced.

Microarray Analysis Reveals Two New Targets of the UPR—The majority of transcripts shown in Fig. 5 and supplemental Table S2 encode proteins with well characterized functions in ER homeostasis, many of which are established targets of the UPR. However, several identified transcripts have not previously been associated with the UPR, and some are derived from open reading frames encoding proteins of unknown function. We, therefore, wanted to investigate whether we could identify new targets of the UPR based on the results of the array analysis. For these studies we chose two candidates: cysteine-rich with EGF-like domain protein 1 (CRELD1) and c18orf45. The former is a predicted membrane-bound homolog of CRELD2, a putative ER protein that is up-regulated by the UPR (46). The latter is an open reading frame encoding a putative GDP-mannose transporter. Both transcripts were significantly up-regulated in response to tunicamycin and thapsigargin as compared with ERp90 and ERLIN1 but only moderately up-regulated compared with BiP and HERP (Fig. 6). As previously shown, the expression level of ERp90 and ERLIN1 is largely unaffected by ER stress, whereas BiP and HERP are strongly up-regulated (47). We concluded that CRELD1 and c18orf45 are novel targets of the mammalian UPR.

DISCUSSION

Maintaining balanced ER redox conditions is fundamentally important for oxidative protein folding to proceed cor-

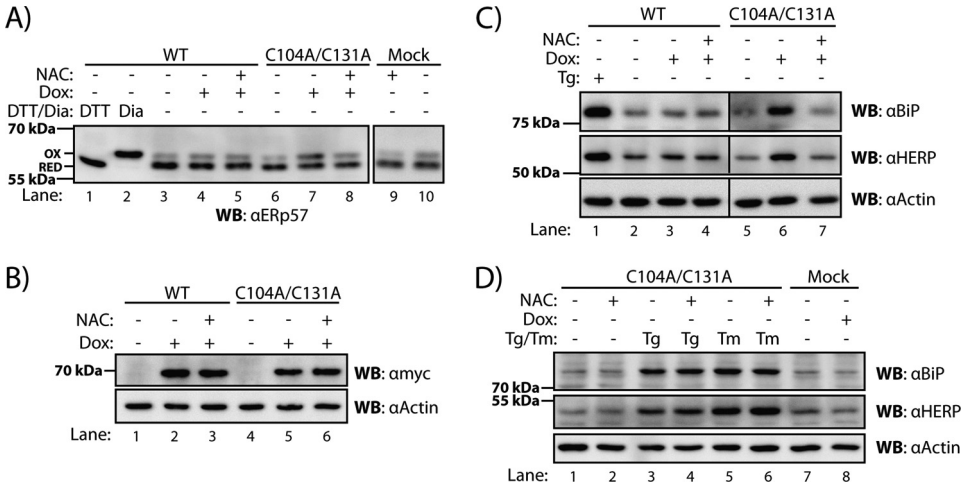

FIGURE 3. **Deregulation of Ero1α perturbs ER redox conditions and induces the UPR.** *A*, where indicated, Ero1α-WT or Ero1α-C104A/C131A cells were induced with dox for 24 h and co-treated with 5 mM NAC for the last 18 h. Before lysis, cells were treated with NEM to alkylate free thiols. After cell lysis, cysteines present in disulfides were reduced and decorated with AMS. Such AMS modification of active-site cysteines originally present in the oxidized state gives rise to slower SDS-PAGE mobility compared with the (NEM-decorated) pool of ERp57 containing reduced active-site cysteines. The cellular redox state of ERp57 was visualized by Western blotting (*WB*). DTT and Diamide (*Dia*)-treated cells were used to show the mobility of fully oxidized (*OX*) and reduced (*RED*) ERp57. *B*, expression levels of Myc-tagged Ero1α variants were analyzed by Western blotting using α-actin as the loading control. *C* and *D*, cells were treated as described for *A*, and the expression levels of BiP and HERP were analyzed by Western blotting using α-actin as the loading control. Cells treated with 5 μM thapsigargin (*Tg*) or 2.5 μg/ml tunicamycin (*Tm*) for 20 h were used to generate positive control lysates for UPR induction.

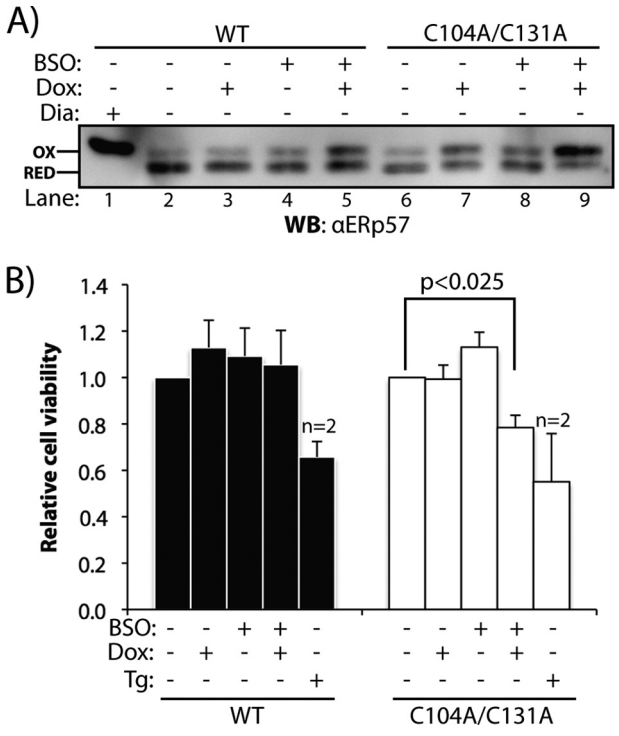

FIGURE 4. **The glutathione redox buffer counteracts Ero1α hyperactivity.** *A*, where indicated, Ero1α-WT or Ero1α-C104A/C131A cells were induced with dox and treated with 1 mM BSO for 24 h. The cellular redox state of ERp57 was visualized by Western blotting (*WB*) as described in Fig. 3*A*. *Dia*, diamide. *B*, cell viability of Ero1α-WT and C104A/C131A cells, which where indicated were treated with dox and/or BSO for 48 h, was assessed by a water-soluble tetrazolium-1 assay (mean ± S.D., $n = 3$). Treatment with 5 μM thapsigargin (*Tg*) for 20 h was used as positive control for cytotoxicity ($n = 2$). Absorbance values were normalized to untreated cells. Statistical significance ($p \leq 0.05$) was assessed by performing Student's unpaired *t* test (two tailed, heteroscedastic) on log 2-transformed -fold changes.

rectly. This study reveals the overall cellular response to an oxidative challenge generated within the ER lumen. The results provide fundamental insight into how maintenance of ER homeostasis depends on the UPR and redox regulation of Ero1α activity.

Using the set of 159 genes with significant changes due to Ero1α overexpression as a basis for further studies, we identified two new targets of the UPR, CRELD1 and c18orf45. Because CRELD1 is a homolog of the known UPR target CRELD2 (46), identification of CRELD1 as a UPR target gene was not unexpected. Unlike c18orf45, CRELD1 appears on the list of 159 genes. To identify c18orf45 as a UPR target, we used another gene present in the set of 159 genes, GDP-mannose pyrophosphorylase A (GMPPA), as a starting point. GDP-mannose pyrophosphorylase A encodes the cytosolic enzyme that generates GDP-mannose from mannose-1-phosphate and GTP. Because the up-regulation of GDP-mannose pyrophosphorylase A indicated an increased demand for GDP-mannose, we decided to test c18orf45 as a potential target of the UPR as this gene is predicted to encode a multispanning membrane protein that shows sequence similarity to the Golgi-resident GDP-mannose transporter 1 (GMT1/VRG4) from *S. cerevisiae* (48). Golgi mannosyltransferases use GDP-mannose precursors as opposed to the mannosyltransferases in the ER, which use the lipid-linked dolichol-P-Man as a saccharide donor (49). This supports the putative function of the protein encoded by c18orf45 as a Golgi-localized GDP-mannose transporter. We expect that further careful data mining of the hits obtained in the array analysis will allow the identification of additional previously unknown UPR targets.

The regulatory disulfides in Ero1p and human Ero1α have proven to be structurally and functionally distinct (50). In Ero1p, the regulatory disulfide bonds likely function to lock the structure in a conformation incompatible with enzymatic activity (51, 52). In Ero1α, two regulatory disulfide bonds have been proposed: Cys^{94}–Cys^{131} and Cys^{99}–Cys^{104} (Fig. 1*A*) (13, 14). By mass spectrometry, we provide the first direct experimental identification of the Cys^{99}–Cys^{104} disulfide bond (Fig. 1, *B* and

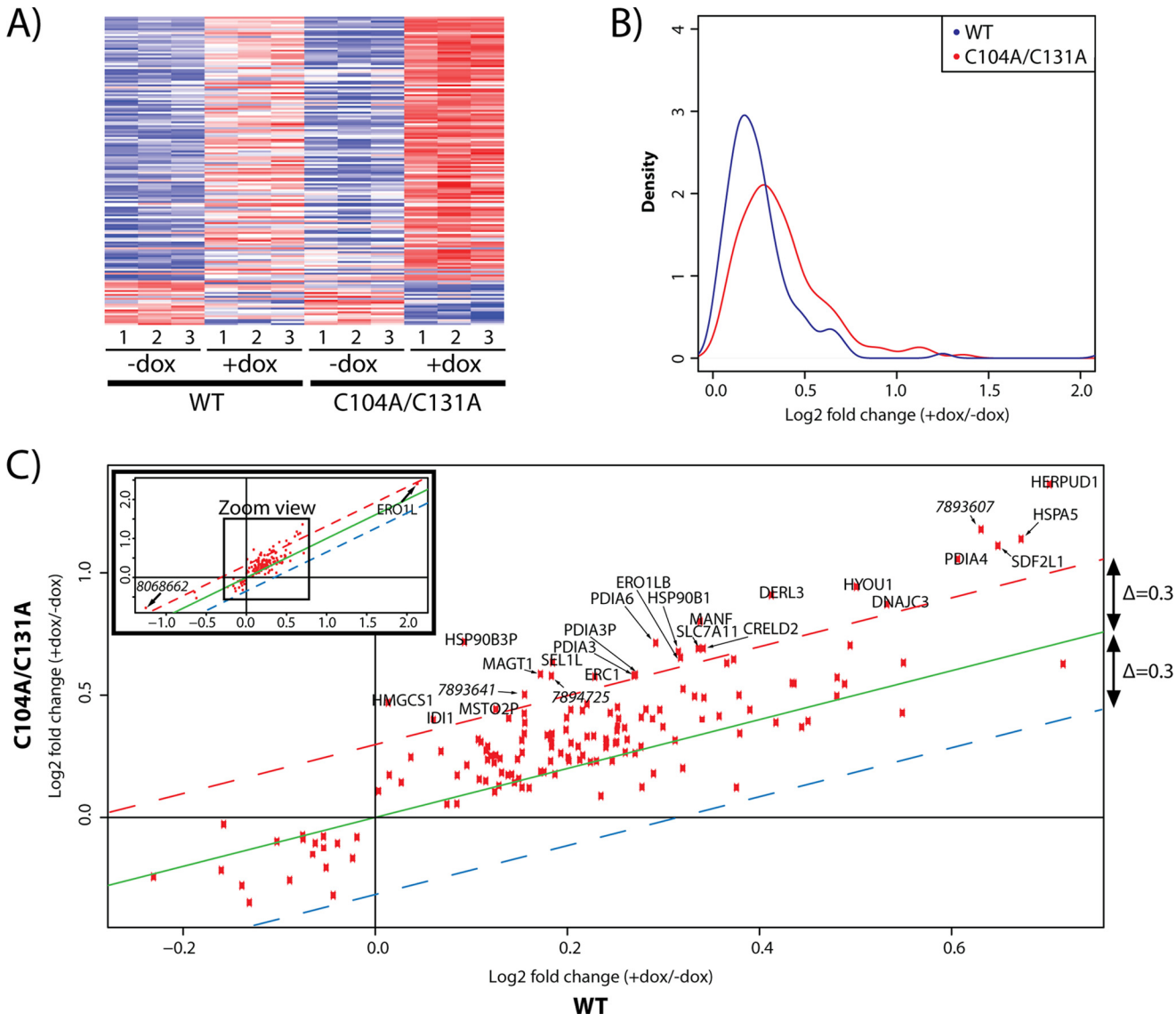

FIGURE 5. **The global transcriptional response to deregulated Ero1α activity.** *A*, shown is a heatmap of the 159 genes found by a two-way analysis of variance to have significant changes in expression levels between non-induced (−*dox*) and induced (+*dox*) cells (see supplemental Table S2). The colors reflect expression intensities (transformed to mean of 0 and S.D. of 1) for each gene, with *red* and *blue colors* corresponding to high and low expression intensities, respectively. Genes are ranked by -fold change (+*dox*/−*dox*) in Ero1α-C104A/C131A cells. *Numbers 1–3* denote independent biological replicates. *B,* shown is a density plot of log 2-transformed -fold changes (+*dox*/−*dox*) in absolute values for the 159 significant genes shown in *A*. *C*, shown is a scatter plot of log 2-transformed -fold changes (+*dox*/−*dox*) of the 159 significant genes in Ero1α-WT and Ero1α-C104A/C131A cells shown in *A* and *B*. Both the full view of the 159 genes (the inserted scatter plot) and an enlarged view (155 genes) are shown. The *green line* indicates no difference in -fold change between Ero1α-WT and Ero1α-C104A/C131A cells, whereas the *dashed red* and *blue lines* signify a difference of 0.3 and −0.3, respectively, between the log 2-transformed -fold changes (+*dox*/−*dox*) for Ero1α-C104A/C131A and Ero1α-WT. For the genes *above the dashed red* lane (see also supplemental Table S3), the associated gene names are either shown on *top of the data point* or in the vicinity of the data point indicated by an *arrow*. Numbers in *italics* denote probeset IDs of unannotated genes.

C, Table 1). This finding shows that regulation of Ero1α activity is indeed based on inactivation of the two outer active-site cysteine residues, which prevents them from forming the Cys^{94}–Cys^{99} disulfide bond for transfer to the substrate.

Based on mobility characteristics under non-reducing conditions of Ero1α Cys-to-Ala mutants, the absence of the Cys^{99}–Cys^{104} regulatory bond was observed to destabilize the other regulatory bond, Cys^{94}–Cys^{131} (Fig. 2, *B* and *C*). A similar regulatory mechanism has been observed in Ero1p, where the presence of one regulatory bond, Cys^{150}–Cys^{295}, protects another, Cys^{143}–Cys^{166}, from reduction (52) and increases the threshold for activation by PDIp (25). As proposed for the yeast system (25), the presence of Ero1α species with different degrees of deregulation could function to fine-tune the activity of the enzyme.

How does the deregulated Ero1α-C104A/C131A mutant turn on the UPR? Induction of the UPR is caused by accumulation of misfolded proteins in the ER (31). Importantly, UPR induction did not seem to be an artifact of overexpressing an ER-localized protein. First, no high molecular weight aggregates were observed for any of the Ero1α Cys-to-Ala mutants (data not shown), suggesting that these mutants did not misfold. Second, the UPR induced by Ero1α-WT was significantly weaker relative to the response induced by Ero1α-C104A/C131A (Fig. 3*C*, supplemental Table S3), although the two proteins were expressed to similar levels (Fig. 3*B*). This

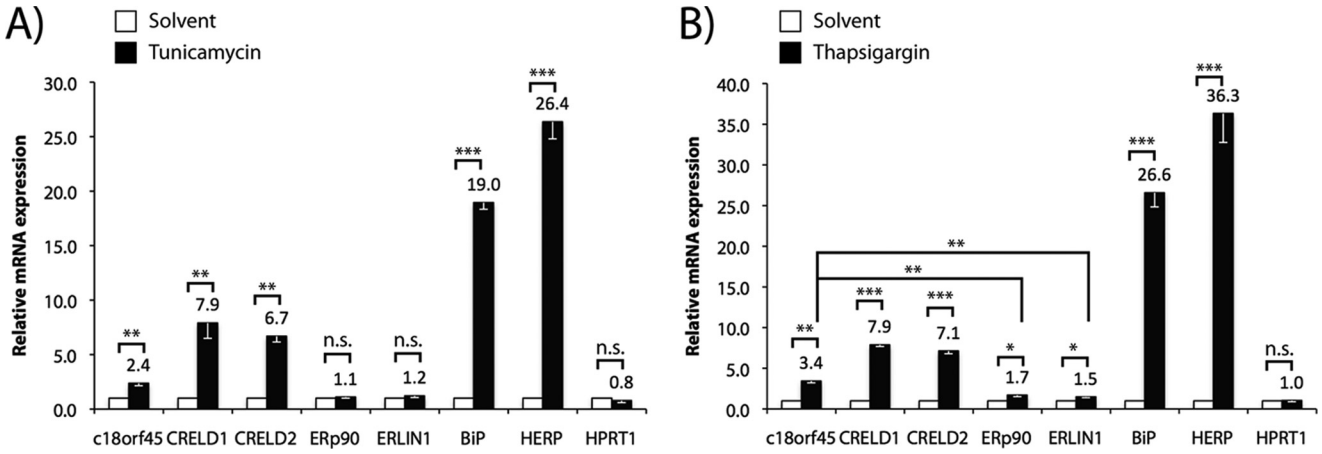

FIGURE 6. **CRELD1, CRELD2, and c18orf45 are transcriptionally up-regulated by the UPR.** *A,* shown is relative abundance of mRNA analyzed by real-time quantitative PCR on RNA extracted from HEK293 cells. Cells were treated with solvent (0.025% DMSO) or 2.5 μg/ml tunicamycin in 0.025% DMSO for 8 h. mRNA levels were normalized to the housekeeping gene GAPDH (mean ± S.D., $n = 3$). ERp90 and ERLIN1 both serve as controls for genes that are largely unaffected by ER stress (47), whereas BiP and HERP serve as positive controls for UPR target genes. The expression level of the housekeeping gene HPRT1 serves as a control for the normalization to GAPDH expression. Statistical significance ($p \leq 0.05$) was assessed by performing Student's unpaired *t* test (two tailed, heteroscedastic) on log 2-transformed -fold changes; *, $p \leq 0.05$; **, $p \leq 0.005$; ***, $p \leq 0.0005$; *n.s.*, not significant. *B,* HEK293 cells were treated with solvent (0.04% ethanol) or 5 μM thapsigargin in 0.04% ethanol for 8 h and analyzed as described in *A*.

shows that overexpression of Ero1 *per se* did not cause a strong UPR. Third, the UPR induction by Ero1α-C104A/C131A was abolished by NAC treatment (Fig. 3*C*), which did not change the expression level of the oxidase (Fig. 3*B*). This demonstrates that the Ero1α-C104A/C131A-generated UPR depends on the hyperoxidizing activity of the mutant rather than its expression level. Importantly, NAC treatment did not have any detectable influence on the UPR induced by thapsigargin and tunicamycin (Fig. 3*D*), indicating that NAC is not a general inhibitor of the UPR.

The observed UPR is likely a result of the high oxidative activity of deregulated Ero1α. Unlike Ero1α-WT, Ero1α-C104A/C131A has been shown to cause H_2O_2-mediated irreversible hyperoxidation of the ER-localized peroxiredoxin IV (PrxIV) in cells (53). One cause for UPR induction by Ero1α-C104A/C131A could, therefore, be H_2O_2-mediated sulf(i/o)nylation of proteins resulting in misfolding. NAC has been shown to directly scavenge hydroxyl radicals but only reacts slowly with H_2O_2 (54). Therefore, direct detoxification of H_2O_2 by NAC (Fig. 3*C*) is probably not the cause of the observed reversion of UPR induction. As GSH is more efficient in scavenging H_2O_2 than NAC (55), a NAC-mediated increase in GSH levels is more likely to explain the effects of NAC, although an indirect function of GSH is also possible (see below).

Ero1α-C104A/C131A overexpression also caused hyperoxidation of ERp57, an effect that was partly abolished by NAC treatment (Fig. 3*A*) and increased by BSO treatment (Fig. 4*A*). When overexpressing Ero1β-C100A/C130A (a hyperactive mutant of Ero1β (10)), very similar results were obtained.[6] Hyperoxidation of ER oxidoreductases could lead to an imbalance in oxidative folding and thereby protein misfolding. Even though ERp57 is a relatively poor substrate of Ero1α as compared with PDI (15), we cannot rule out an increased direct oxidation of ERp57 by Ero1α-C104A/C131A. However, the primary cause of hyperoxidation of ERp57 is likely an elevated glutathione reduction potential (*i.e.* more oxidizing conditions) in the ER. Previously, we showed that overexpression of Ero1α-C131A leads to an increase in the ratio between GSSG and total glutathione (13). We expect the same effect for Ero1α-C104A/C131A, as overexpression of this mutant leads to a slightly more pronounced effect on ERp57 hyperoxidation relative to Ero1α-C131A (data not shown). Overexpression of Ero1β-C100A/C130A also increases the ER glutathione reduction potential as measured by a glutathione-specific fluorescence-based sensor.[7] Similarly, an increased luminal GSSG:GSH ratio has been demonstrated upon stimulation of H_2O_2 production in the ER by a system based on gulonolactone oxidase (56).

An increased glutathione reduction potential would normally inactivate Ero1α and Ero1p through feedback regulation via PDI (1, 25). In accordance, an observed growth inhibition of yeast cells mediated by the hyperactive Ero1p-C150A/C295A mutant was alleviated by BSO treatment (51). Upon BSO-mediated depletion of GSH, Ero1p-C150A/C295A was predominantly in an oxidized redox state, suggesting that Ero1p was inactivated by the formation of another regulatory intramolecular disulfide bond (51). Because the Cys^{143}–Cys^{166} disulfide is destabilized by the absence of the Cys^{150}–Cys^{295} disulfide (52), the Cys^{143}–Cys^{166} disulfide is potentially reformed upon BSO treatment and thereby inactivates Ero1p-C150A/C295A. On the contrary, cell viability was reduced in cells overexpressing Ero1α-C104A/C131A only when the glutathione redox buffer was compromised by BSO (Fig. 4*B*). This indicates that an inactivation process similar to the one occurring in Ero1p-C150A/C295A was not possible in Ero1α-C104A/C131A. This is consistent with the fact that both cysteines (Cys^{104} and Cys^{131}) engaged in the regulatory disulfide bonds with the outer active-site cysteines (Cys^{94} and Cys^{99}) were absent (Fig. 2*C*).

Based on the shown effects of Ero1α-C104A/C131A hyperactivity, it is intriguing that the array analysis did not reveal a

[6] H. G. Hansen and L. Ellgaard, unpublished observations.

[7] J. Birk, M. Meyer, H. G. Hansen, A. Odermatt, T. P. Dick, and C. Appenzeller-Herzog, manuscript submitted.

broad transcriptional up-regulation of genes involved in antioxidant responses. Transcripts of ER-resident enzymes with the potential to scavenge H_2O_2, peroxiredoxin IV (53, 57), and glutathione peroxidases 7 and 8 (58) were not up-regulated, and only three genes of the GO term "Response to oxidative stress" were identified among the top 159 significant genes: SELK, DHCR24, and SLC7A11. Among these, the most direct connection to the effects elicited by Ero1α-C104A/C131A overexpression was found for the SLC7A11 gene. This gene also appears on the list of 26 genes with considerably higher relative -fold changes between Ero1α-C104A/131A (+dox/−dox) and Ero1α-WT (+dox/−dox) (supplemental Table S3). The SLC7A11 gene encodes the substrate-specific subunit (xCT) of the heterodimeric plasmamembrane cystine/glutamate antiporter, x_C^-. The cystine imported by x_C^- is reduced to cysteine, which is then used for GSH synthesis (59). Moreover, overexpression of xCT rescues GSH deficiency in cells devoid of γ-glutamylcysteine synthase, which catalyzes the rate-limiting step in GSH synthesis (60). During B-cell differentiation, where an increased production of H_2O_2 originating from various sources is observed, xCT is up-regulated as part of a broad antioxidant response (61).

Together with the observed effects of treating cells overexpressing Ero1α-C104A/C131A with NAC and BSO, the up-regulation of the SLC7A11 gene indicates xCT to counteract an oxidizing imbalance in the ER glutathione redox buffer through cytosolic import of cystine, an essential building block for the synthesis of GSH.

The nuclear erythroid 2 p45-related factor 2 (Nrf2) transcription factor controls the expression of a number of antioxidant response genes (62). However, our transcriptome analysis did not demonstrate an obvious activation of the Nrf2-mediated antioxidant response. As this response is triggered by ROS accumulation in the cytosol (62), we suggest that the vast majority of Ero1α-C104A/C131A-derived H_2O_2 is confined to the ER. Here GSH could either directly detoxify H_2O_2 or indirectly detoxify by buffering the redox state of protein disulfide isomerases. Thus, we propose that Ero1α-C104A/C131A overexpression elicits NAC-sensitive ER stress through local hyperoxidation and does not cause broad oxidative injury throughout the cell.

Acknowledgments—We thank Z. Nikrozi, N. P. Jensen, and K. Doherty for technical assistance, J. Vikesaa from the RH Microarray Center (Copenhagen) for help with preliminary analysis of the gene expression profiling data, Linda Hendershot and Ari Helenius for providing antibodies, and all members of the Ellgaard lab for critical reading of the manuscript.

REFERENCES

1. Appenzeller-Herzog, C., Riemer, J., Zito, E., Chin, K. T., Ron, D., Spiess, M., and Ellgaard, L. (2010) Disulphide production by Ero1α-PDI relay is rapid and effectively regulated. *EMBO J.* **29,** 3318–3329
2. Rutkevich, L. A., and Williams, D. B. (2012) Vitamin K epoxide reductase contributes to protein disulfide formation and redox homeostasis within the endoplasmic reticulum. *Mol. Biol. Cell* **23,** 2017–2027
3. Cabibbo, A., Pagani, M., Fabbri, M., Rocchi, M., Farmery, M. R., Bulleid, N. J., and Sitia, R. (2000) ERO1-L, a human protein that favors disulfide bond formation in the endoplasmic reticulum. *J. Biol. Chem.* **275,** 4827–4833
4. Pagani, M., Fabbri, M., Benedetti, C., Fassio, A., Pilati, S., Bulleid, N. J., Cabibbo, A., and Sitia, R. (2000) Endoplasmic reticulum oxidoreductin 1-lβ (ERO1-Lβ), a human gene induced in the course of the unfolded protein response. *J. Biol. Chem.* **275,** 23685–23692
5. Dias-Gunasekara, S., Gubbens, J., van Lith, M., Dunne, C., Williams, J. A., Kataky, R., Scoones, D., Lapthorn, A., Bulleid, N. J., and Benham, A. M. (2005) Tissue-specific expression and dimerization of the endoplasmic reticulum oxidoreductase Ero1β. *J. Biol. Chem.* **280,** 33066–33075
6. Tu, B. P., and Weissman, J. S. (2002) The FAD- and O_2-dependent reaction cycle of Ero1-mediated oxidative protein folding in the endoplasmic reticulum. *Mol. Cell* **10,** 983–994
7. Mezghrani, A., Fassio, A., Benham, A., Simmen, T., Braakman, I., and Sitia, R. (2001) Manipulation of oxidative protein folding and PDI redox state in mammalian cells. *EMBO J.* **20,** 6288–6296
8. Wang, L., Li, S. J., Sidhu, A., Zhu, L., Liang, Y., Freedman, R. B., and Wang, C. C. (2009) Reconstitution of human Ero1-Lα/protein-disulfide isomerase oxidative folding pathway *in vitro*. Position-dependent differences in role between the a and a′ domains of protein-disulfide isomerase. *J. Biol. Chem.* **284,** 199–206
9. Gross, E., Sevier, C. S., Heldman, N., Vitu, E., Bentzur, M., Kaiser, C. A., Thorpe, C., and Fass, D. (2006) Generating disulfides enzymatically. Reaction products and electron acceptors of the endoplasmic reticulum thiol oxidase Ero1p. *Proc. Natl. Acad. Sci. U.S.A.* **103,** 299–304
10. Wang, L., Zhu, L., and Wang, C. C. (2011) The endoplasmic reticulum sulfhydryl oxidase Ero1β drives efficient oxidative protein folding with loose regulation. *Biochem. J.* **434,** 113–121
11. Bulleid, N. J., and Ellgaard, L. (2011) Multiple ways to make disulfides. *Trends Biochem. Sci.* **36,** 485–492
12. Araki, K., and Nagata, K. (2011) Functional *in vitro* analysis of the ERO1 protein and protein-disulfide isomerase pathway. *J. Biol. Chem.* **286,** 32705–32712
13. Appenzeller-Herzog, C., Riemer, J., Christensen, B., Sørensen, E. S., and Ellgaard, L. (2008) A novel disulphide switch mechanism in Ero1α balances ER oxidation in human cells. *EMBO J.* **27,** 2977–2987
14. Baker, K. M., Chakravarthi, S., Langton, K. P., Sheppard, A. M., Lu, H., and Bulleid, N. J. (2008) Low reduction potential of Ero1α regulatory disulphides ensures tight control of substrate oxidation. *EMBO J.* **27,** 2988–2997
15. Inaba, K., Masui, S., Iida, H., Vavassori, S., Sitia, R., and Suzuki, M. (2010) Crystal structures of human Ero1α reveal the mechanisms of regulated and targeted oxidation of PDI. *EMBO J.* **29,** 3330–3343
16. Bertoli, G., Simmen, T., Anelli, T., Molteni, S. N., Fesce, R., and Sitia, R. (2004) Two conserved cysteine triads in human Ero1α cooperate for efficient disulfide bond formation in the endoplasmic reticulum. *J. Biol. Chem.* **279,** 30047–30052
17. Benham, A. M., Cabibbo, A., Fassio, A., Bulleid, N., Sitia, R., and Braakman, I. (2000) The C*XXCXX*C motif determines the folding, structure, and stability of human Ero1-Lα. *EMBO J.* **19,** 4493–4502
18. Chakravarthi, S., Jessop, C. E., and Bulleid, N. J. (2006) The role of glutathione in disulphide bond formation and endoplasmic-reticulum-generated oxidative stress. *EMBO Rep.* **7,** 271–275
19. Appenzeller-Herzog, C. (2011) Glutathione- and non-glutathione-based oxidant control in the endoplasmic reticulum. *J. Cell Sci.* **124,** 847–855
20. Hwang, C., Sinskey, A. J., and Lodish, H. F. (1992) Oxidized redox state of glutathione in the endoplasmic reticulum. *Science* **257,** 1496–1502
21. Chakravarthi, S., and Bulleid, N. J. (2004) Glutathione is required to regulate the formation of native disulfide bonds within proteins entering the secretory pathway. *J. Biol. Chem.* **279,** 39872–39879
22. Molteni, S. N., Fassio, A., Ciriolo, M. R., Filomeni, G., Pasqualetto, E., Fagioli, C., and Sitia, R. (2004) Glutathione limits Ero1-dependent oxidation in the endoplasmic reticulum. *J. Biol. Chem.* **279,** 32667–32673
23. Tu, B. P., Ho-Schleyer, S. C., Travers, K. J., and Weissman, J. S. (2000) Biochemical basis of oxidative protein folding in the endoplasmic reticulum. *Science* **290,** 1571–1574
24. Sevier, C. S., and Kaiser, C. A. (2006) Disulfide transfer between two conserved cysteine pairs imparts selectivity to protein oxidation by Ero1. *Mol. Biol. Cell* **17,** 2256–2266
25. Kim, S., Sideris, D. P., Sevier, C. S., and Kaiser, C. A. (2012) Balanced Ero1

activation and inactivation establishes ER redox homeostasis. *J. Cell Biol.* **196,** 713–725
26. Braakman, I., Helenius, J., and Helenius, A. (1992) Manipulating disulfide bond formation and protein folding in the endoplasmic reticulum. *EMBO J.* **11,** 1717–1722
27. Merksamer, P. I., Trusina, A., and Papa, F. R. (2008) Real-time redox measurements during endoplasmic reticulum stress reveal interlinked protein folding functions. *Cell* **135,** 933–947
28. Garg, A. D., Krysko, D. V., Verfaillie, T., Kaczmarek, A., Ferreira, G. B., Marysael, T., Rubio, N., Firczuk, M., Mathieu, C., Roebroek, A. J., Annaert, W., Golab, J., de Witte, P., Vandenabeele, P., and Agostinis, P. (2012) A novel pathway combining calreticulin exposure and ATP secretion in immunogenic cancer cell death. *EMBO J.* **31,** 1062–1079
29. Kaufman, R. J., Back, S. H., Song, B., Han, J., and Hassler, J. (2010) The unfolded protein response is required to maintain the integrity of the endoplasmic reticulum, prevent oxidative stress, and preserve differentiation in β-cells. *Diabetes Obes. Metab.* **12,** 99–107
30. Travers, K. J., Patil, C. K., Wodicka, L., Lockhart, D. J., Weissman, J. S., and Walter, P. (2000) Functional and genomic analyses reveal an essential coordination between the unfolded protein response and ER-associated degradation. *Cell* **101,** 249–258
31. Walter, P., and Ron, D. (2011) The unfolded protein response. From stress pathway to homeostatic regulation. *Science* **334,** 1081–1086
32. Hetz, C. (2012) The unfolded protein response. Controlling cell fate decisions under ER stress and beyond. *Nat. Rev. Mol. Cell Biol.* **13,** 89–102
33. Back, S. H., and Kaufman, R. J. (2012) Endoplasmic reticulum stress and type 2 diabetes. *Annu. Rev. Biochem.* **81,** 767–793
34. Harding, H. P., Zhang, Y., Zeng, H., Novoa, I., Lu, P. D., Calfon, M., Sadri, N., Yun, C., Popko, B., Paules, R., Stojdl, D. F., Bell, J. C., Hettmann, T., Leiden, J. M., and Ron, D. (2003) An integrated stress response regulates amino acid metabolism and resistance to oxidative stress. *Mol. Cell* **11,** 619–633
35. Hsieh, Y. H., Su, I. J., Lei, H. Y., Lai, M. D., Chang, W. W., and Huang, W. (2007) Differential endoplasmic reticulum stress signaling pathways mediated by iNOS. *Biochem. Biophys. Res. Commun.* **359,** 643–648
36. Malhotra, J. D., Miao, H., Zhang, K., Wolfson, A., Pennathur, S., Pipe, S. W., and Kaufman, R. J. (2008) Antioxidants reduce endoplasmic reticulum stress and improve protein secretion. *Proc. Natl. Acad. Sci. U.S.A.* **105,** 18525–18530
37. Appenzeller-Herzog, C., and Ellgaard, L. (2008) *In vivo* reduction-oxidation state of protein disulfide isomerase. The two active sites independently occur in the reduced and oxidized forms. *Antioxid. Redox Signal.* **10,** 55–64
38. Livak, K. J., and Schmittgen, T. D. (2001) Analysis of relative gene expression data using real-time quantitative PCR and the $2(-\Delta\Delta C(T))$ method. *Methods* **25,** 402–408
39. Irizarry, R. A., Bolstad, B. M., Collin, F., Cope, L. M., Hobbs, B., and Speed, T. P. (2003) Summaries of Affymetrix GeneChip probe level data. *Nucleic Acids Res.* **31,** e15
40. Maere, S., Heymans, K., and Kuiper, M. (2005) BiNGO. A Cytoscape plugin to assess overrepresentation of gene ontology categories in biological networks. *Bioinformatics* **21,** 3448–3449
41. Jessop, C. E., and Bulleid, N. J. (2004) Glutathione directly reduces an oxidoreductase in the endoplasmic reticulum of mammalian cells. *J. Biol. Chem.* **279,** 55341–55347
42. Zafarullah, M., Li, W. Q., Sylvester, J., and Ahmad, M. (2003) Molecular mechanisms of *N*-acetylcysteine actions. *Cell. Mol. Life Sci.* **60,** 6–20
43. Kolossov, V. L., Leslie, M. T., Chatterjee, A., Sheehan, B. M., Kenis, P. J., and Gaskins, H. R. (2012) Forster resonance energy transfer-based sensor targeting endoplasmic reticulum reveals highly oxidative environment. *Exp. Biol. Med.* (*Maywood*) **237,** 652–662
44. Zhang, H., Limphong, P., Pieper, J., Liu, Q., Rodesch, C. K., Christians, E., and Benjamin, I. J. (2012) Glutathione-dependent reductive stress triggers mitochondrial oxidation and cytotoxicity. *FASEB J.* **26,** 1442–1451
45. Yamamoto, K., Sato, T., Matsui, T., Sato, M., Okada, T., Yoshida, H., Harada, A., and Mori, K. (2007) Transcriptional induction of mammalian ER quality control proteins is mediated by single or combined action of ATF6α and XBP1. *Dev. Cell* **13,** 365–376
46. Oh-hashi, K., Koga, H., Ikeda, S., Shimada, K., Hirata, Y., and Kiuchi, K. (2009) CRELD2 is a novel endoplasmic reticulum stress-inducible gene. *Biochem. Biophys. Res. Commun.* **387,** 504–510
47. Christianson, J. C., Olzmann, J. A., Shaler, T. A., Sowa, M. E., Bennett, E. J., Richter, C. M., Tyler, R. E., Greenblatt, E. J., Harper, J. W., and Kopito, R. R. (2012) Defining human ERAD networks through an integrative mapping strategy. *Nat. Cell Biol.* **14,** 93–105
48. Dean, N., Zhang, Y. B., and Poster, J. B. (1997) The VRG4 gene is required for GDP-mannose transport into the lumen of the Golgi in the yeast, *Saccharomyces cerevisiae*. *J. Biol. Chem.* **272,** 31908–31914
49. Helenius, A., and Aebi, M. (2004) Roles of N-linked glycans in the endoplasmic reticulum. *Annu. Rev. Biochem.* **73,** 1019–1049
50. Tavender, T. J., and Bulleid, N. J. (2010) Molecular mechanisms regulating oxidative activity of the Ero1 family in the endoplasmic reticulum. *Antioxid. Redox Signal.* **13,** 1177–1187
51. Sevier, C. S., Qu, H., Heldman, N., Gross, E., Fass, D., and Kaiser, C. A. (2007) Modulation of cellular disulfide-bond formation and the ER redox environment by feedback regulation of Ero1. *Cell* **129,** 333–344
52. Heldman, N., Vonshak, O., Sevier, C. S., Vitu, E., Mehlman, T., and Fass, D. (2010) Steps in reductive activation of the disulfide-generating enzyme Ero1p. *Protein Sci.* **19,** 1863–1876
53. Tavender, T. J., and Bulleid, N. J. (2010) Peroxiredoxin IV protects cells from oxidative stress by removing H_2O_2 produced during disulphide formation. *J. Cell Sci.* **123,** 2672–2679
54. Aruoma, O. I., Halliwell, B., Hoey, B. M., and Butler, J. (1989) The antioxidant action of N-acetylcysteine. Its reaction with hydrogen peroxide, hydroxyl radical, superoxide, and hypochlorous acid. *Free Radic. Biol. Med.* **6,** 593–597
55. Winterbourn, C. C., and Metodiewa, D. (1999) Reactivity of biologically important thiol compounds with superoxide and hydrogen peroxide. *Free Radic. Biol. Med.* **27,** 322–328
56. Margittai, É., Löw, P., Stiller, I., Greco, A., Garcia-Manteiga, J. M., Pengo, N., Benedetti, A., Sitia, R., and Bánhegyi, G. (2012) Production of H_2O_2 in the endoplasmic reticulum promotes *in vivo* disulfide bond formation. *Antioxid. Redox Signal.* **16,** 1088–1099
57. Zito, E., Melo, E. P., Yang, Y., Wahlander, Å., Neubert, T. A., and Ron, D. (2010) Oxidative protein folding by an endoplasmic reticulum-localized peroxiredoxin. *Mol. Cell* **40,** 787–797
58. Nguyen, V. D., Saaranen, M. J., Karala, A. R., Lappi, A. K., Wang, L., Raykhel, I. B., Alanen, H. I., Salo, K. E., Wang, C. C., and Ruddock, L. W. (2011) Two endoplasmic reticulum PDI peroxidases increase the efficiency of the use of peroxide during disulfide bond formation. *J. Mol. Biol.* **406,** 503–515
59. Bannai, S., and Tateishi, N. (1986) Role of membrane transport in metabolism and function of glutathione in mammals. *J. Membr. Biol.* **89,** 1–8
60. Mandal, P. K., Seiler, A., Perisic, T., Kölle, P., Banjac Canak, A., Förster, H., Weiss, N., Kremmer, E., Lieberman, M. W., Bannai, S., Kuhlencordt, P., Sato, H., Bornkamm, G. W., and Conrad, M. (2010) System x(c)- and thioredoxin reductase 1 cooperatively rescue glutathione deficiency. *J. Biol. Chem.* **285,** 22244–22253
61. Vené, R., Delfino, L., Castellani, P., Balza, E., Bertolotti, M., Sitia, R., and Rubartelli, A. (2010) Redox remodeling allows and controls B-cell activation and differentiation. *Antioxid. Redox Signal.* **13,** 1145–1155
62. Itoh, K., Mimura, J., and Yamamoto, M. (2010) Discovery of the negative regulator of Nrf2, Keap1. A historical overview. *Antioxid. Redox Signal.* **13,** 1665–1678